Toward a Unified Multiresolution Scheme in the Combined Physical/Stochastic Space for Stochastic Differential Equations

Remi Abgrall, Pietro Marco Congedo, Gianluca Geraci

Toward a Unified Multiresolution Scheme in the Combined Physical/Stochastic Space for Stochastic Differential Equations

Remi Abgrall, Pietro Marco Congedo, Gianluca Geraci

RESEARCH REPORT
N° 7996
June 18, 2012
Project-Team Bacchus

ISSN 0249-6399 ISRN INRIA/RR--7996--FR+ENG

Toward a Unified Multiresolution Scheme in the Combined Physical/Stochastic Space for Stochastic Differential Equations

Remi Abgrall, Pietro Marco Congedo, Gianluca Geraci

Project-Team Bacchus

Research Report n° 7996 — June 18, 2012 — 23 pages

Abstract: In the present work, an innovative method for solving stochastic partial differential equations is presented. A multiresolution method permitting to compute statistics of the quantity of interest for a whatever form of the probability density function is extended to permit an adaptation in both physical and stochastic spaces. The efficiency of this strategy, in terms of refinement/derefinement capabilities, is displayed for stochastic algebraic and differential equations with respect to other more classical techniques, like Monte Carlo (MC) and Polynomial Chaos (PC). Finally, the proposed strategy is applied to the heat equation, displaying very promising results in terms of accuracy, convergence and regularity.

Key-words: Multiresolution, Ordinary Differential Equations, Partial Differential Equation, Uncertainty Quantification, Heat Equation.

RESEARCH CENTRE
BORDEAUX – SUD-OUEST

351, Cours de la Libération
Bâtiment A 29
33405 Talence Cedex

Schéma multirésolution pour la résolution d'équations différentielles stochastiques dans l'espace couplé physique/stochastique

Résumé : Dans cette étude, on présente une méthode innovante pour résoudre les équations aux dérivées partielles stochastiques. Une méthode, précédemment développée afin de calculer une quantité d'intérêt pour une fonction densité de probabilité quelconque, est étendue pour permettre l'adaptation dans les espaces physiques et stochastiques en même temps. L'efficacité de cette stratégie, en terme de capacité à raffiner/déraffiner, est démontrée sur des équations algébriques et différentielles par rapport à d'autres techniques plus classiques, tel que Monte Carlo et Chaos Polynomial. Enfin, cette stratégie est appliquée à l'équation de la chaleur avec des résultats très prometteurs en terme de précision, convergence et régularité.

Mots-clés : Multirésolution, équations différentielles ordinaires, équation aux dérivées partielles, quantification de l'incertitude, équation de la chaleur.

1. Introduction

In the last fifty years, a strong effort has been devoted to develop efficient numerical methods for solving partial differential equations. Estimating the predictivity of a numerical simulation remains very challenging. One of the most important issues is that the physical model and/or the initial/boundary conditions are strongly affected by uncertainties. A general agreement is reached on the necessity to take into account experimental and modeling uncertainties in the numerical simulation. The so-called Uncertainty Quantification (UQ) is a branch of the numerical analysis that has been developed more recently to quantify the uncertainty and to estimate the confidence interval of a certain quantity of interest.

The first and most known UQ method is the Monte Carlo method. The Polynomial Chaos (PC) techniques has acquired great popularity in last years. In the original work of Wiener [1], the solution is expanded in a polynomial Hermite basis, the so-called homogeneous chaos expansion, while in recent years, Xiu and Karniadakis [2] demonstrated that the optimal convergence can be achieved if orthogonal basis are chosen following the so-called Wiener-Askey scheme. This leads to the well-known generalized Polynomial Chaos (gPC) approach. However, problems with discontinuities in the random space can lead to slow convergence. Similarly, long-time integration problems could be encountered [3], where this behavior is due to the modification in time of the statistic properties of the solution inducing an efficiency loss of the polynomial basis in time. Recently, Gerritsma [4] proposed a time-dependent generalized Polynomial Chaos scheme based on the research of a time varying optimal polynomial basis. The majors drawbacks related to the application of the PC to real-like cases is related to the presence of discontinuities, in both physical and stochastic spaces, to long-time integration problems and to the use of a custom-defined form of probability density function (for example discontinuous and unsteady). Actually, handling a discontinuity in both physical and stochastic spaces remains a very challenging issue. In the context of gPC schemes, Wan and Karniadakis introduced an adaptive class of methods for solving discontinuities by using local basis functions, the multi-element generalized Polynomial Chaos (ME-gPC) [5]. This strategy deals with an adaptive decomposition of the domain on which local basis are employed. In order to treat discontinuous response surfaces, Le Maître et al. applied a multiresolution analysis to Galerkin projection schemes [6, 7, 8]. This class of schemes relies on the projection of the uncertain data on a multi-wavelets basis consisting of piecewise polynomial (smooth) functions. This approach is shown to be very CPU demanding. Consequently, two cures are then explored in the context of adaptive methods: automatically refine the multi-wavelets basis or adaptively partitioning the domain.

More recently, Abgrall et al. [9, 10, 11] introduces a new class of finite volume schemes capable to deal with discontinuous problems for shock-dominated flows. The so called semi-intrusive scheme (SI) exhibits promising results in term of accuracy and efficiency compared to more classical Monte Carlo and PC methods. A step-forward for reducing the computational cost and preserving accuracy is made by the authors with a new technique inspired to the Multiresolution framework of Harten [12, 13, 14]. Preliminary results in this direction [15], for problems with custom-defined probability density functions, displays promising results with respect to classical techniques like MC and PC.

In this work, this method is extended to solve not only ordinary differential equations, as made in [15] using the Truncate and Encode (TE) technique, but also partial differential equations. A new stochastic technique, called spatial-TE (sTE), is presented with refinement/derefinement capabilities in time for both the physical and stochastic spaces. The main advantage is the overall reduction of the total number of points needed to reach a certain level of accuracy for the complete stochastic solution.

The approach proposed in the present work is based on a multiresolution concept, as already made in Le Maître et al. [8]. Anyway, the approach differs completely since here no spectral projection is employed, as it will be explained in the next section. Moreover, the possibility to reject a wavelets (equal to an interpolation error as in the original Harten framework) is based only on local tests, then is different from Galerkin projection approach where 1D energy estimators along stochastic dimensions are used. For details on the multiresolution approach applied to Galerkin projection schemes, the reader can refer to the extremely exhaustive reference [16].

This paper is organized as follows. In Section 2, the mathematical problem is defined. The new strategy, *i.e.* the sTE, is illustrated in Section 3. Then, the application to the stochastic heat equation is presented in Section 4. Section 5 presents several numerical results for different test-cases. Finally, some conclusions and perspectives are drawn in Section 6.

2. Mathematical setting

Consider the following problem for an output of interest $u(\mathbf{x}, t, \boldsymbol{\xi}(\omega))$[1]:

$$\mathcal{L}(\mathbf{x}, t, \boldsymbol{\xi}(\omega); u(\mathbf{x}, t, \boldsymbol{\xi}(\omega))) = \mathcal{S}(\mathbf{x}, t, \boldsymbol{\xi}(\omega)), \tag{1}$$

where the operator $\mathcal{L}$ can be either an algebraic or a differential operator (in this case we need appropriate initial and boundary conditions). The operator $\mathcal{L}$ and the source term $\mathcal{S}$ are defined on the domain $D \times T \times \Xi$, where $\mathbf{x} \in D \subset \mathbb{R}^{n_d}$, with $n_d \in \{1, 2, 3\}$, and $t \in T$ are the spatial and temporal dimensions. Randomness is introduced in (1) and its initial and boundary conditions in term of d second order random parameters $\boldsymbol{\xi}(\omega) = \{\xi_1(\omega_1), \ldots, \xi_d(\omega_d)\} \in \Xi$ with parameter space $\Xi \subset \mathbb{R}^d$. The symbol $\omega = \{\omega_1, \ldots, \omega_d\} \in \Omega \subset \mathbb{R}$ denotes realizations in a complete probability space $(\Omega, \mathcal{F}, P)$. Here Ω is the set of outcomes, $\mathcal{F} \subset 2^\Omega$ is the σ-algebra of events and $P : \mathcal{F} \to [0, 1]$ is a probability measure. In our case the random variables ω are by definition standard uniformly $\mathcal{U}(0, 1)$ distributed. Random parameters $\boldsymbol{\xi}(\omega)$ can have any arbitrary probability density function $p(\boldsymbol{\xi}(\omega))$, in this way $p(\boldsymbol{\xi}(\omega)) > 0$ for all $\boldsymbol{\xi}(\omega) \in \Xi$ and $p(\boldsymbol{\xi}(\omega)) = 0$ for all $\boldsymbol{\xi}(\omega) \notin \Xi$; we can now drop the argument ω for brevity. The probability density function $p(\boldsymbol{\xi}(\omega))$ is defined as a joint probability density function from the independent probability function of each variable: $p(\boldsymbol{\xi}(\omega)) = \prod_{i=1}^{d} p_i(\xi_i)$. This assumption allows an independent polynomial representation for each direction in the probabilistic space with the possibility to recover the multidimensional representation by tensorization. The aim of UQ is to find the statistical moments of the solution $u(\boldsymbol{\xi})$.

3. The spatial-TE (sTE) strategy

The aim of the present work is to propose an efficient strategy to solve efficiently stochastic partial differential equation.

In [15], we presented a technique inspired to the classical multiresolution framework of Harten [13, 14], but adapted to the computation of statistics in the stochastic space Ξ in the case of time dependent and eventually discontinuous probability density functions. This so-called truncate and encode strategy (TE) can be employed to obtain non-intrusive solutions in the case of problems defined only in the stochastic space. This basic algorithm is briefly presented in Section 3.1 and 3.2, where the strategy describing the evolution in time is shown.

In this paper, we show how this algorithm could be extended in order to solve stochastic partial differential equation. A detailed description of this new algorithm is then illustrated in Section 3.3.

3.1. The Truncate and Encode strategy

Here, for simplicity, only the 1D case with uniform distribution of points is considered, even if the same conclusions hold for higher dimensional meshes of non structured type (see [17]). In the following, we indicate the generic mesh level k of N_k equally spaced intervals of length h_k as

$$\mathcal{G}^k = \left\{\xi_j^k\right\}_{j=0}^{N_k}, \quad \xi_j^k = jh_k, \quad h_k = 2^k h_0, \quad N_k = N_0/2^k.$$

A representation of the solution on a finest grid is computed starting from a coarsest grid, with a lower number of evaluation of the function (in the space Ξ). The remaining points can be obtained by interpolation under the hypothesis to make an error that can be driven by a threshold parameter ε. The Harten framework consists of three different steps:

- Encoding: the solution represented on the finest mesh $\mathcal{G}^0$ is employed to obtain a hierarchical representation on a nested sequence of levels $k = 1, \ldots, L$ where $\mathcal{G}^k$ are obtained directly from $\mathcal{G}^{k-1}$ without considering the odd points. For each *missing point* $\xi_j^k \in \mathcal{G}^{k+1} - \mathcal{G}^k$, a *detail* or *wavelet* is computed as $d_j^k = u_{2j-1}^{k-1} - \tilde{u}_{2j-1}^{k-1}$, where $\tilde{u}_{2j-1}^{k-1}$ is an approximation of the value employing a whatever interpolation operator $\mathcal{I}(\xi; u^k)$ that interpolates the function u on the level k in the point ξ. In the present work, we have chosen, in order to simplify the exposure, the simplest example, namely a linear interpolation operator. However, the extension to more complex and

[1] In the following the exposition is made for a scalar output variable (u) for brevity, but the extension to the multidimensional output case is straightforward.

more accurate interpolation would lead to similar algorithms. The final result of the *encoding* procedure is to obtain a multiresolution u_M representation of u: $(u_M)^{\mathrm{T}} = (d^1, d^2, \ldots, d^L, u^L)$ where $d^k = \{d_j^k\}$ and $k = L$ is the coarsest level. For brevity, the procedure can be re-arranged in matrix form: $u_M = Mu^0$.

- Truncation: to obtain a data compression of the solution at the finest level $\hat{u}^0$, a threshold can be introduced to eliminate the non-significant *wavelets*. In particular, a truncated *detail* is defined as follows

$$\hat{d}_j^k = \begin{cases} d_j^k & \text{if} \quad |d_j^k| > \varepsilon_k \\ 0 & \text{if} \quad |d_j^k| \leq \varepsilon_k. \end{cases} \tag{2}$$

  As a consequence, the truncated multiresolution representation consists in $\hat{u}_M = (\hat{d}^1, \hat{d}^2, \ldots, \hat{d}^L, u^L)$.

- Decoding: once the truncation is performed, the solution on the finest level can be obtained directly from the coarsest one $\hat{u}^0 = M^{-1}\hat{u}_M$. The following estimation holds (see [12] for a proof)

$$\|u^0 - \hat{u}^0\| \leq C\varepsilon, \tag{3}$$

  if $\varepsilon_k = \varepsilon/2$.

Now, we can introduce our procedure permitting to perform the encoding and truncation procedure at the same time starting from the coarsest level to the finest. This is necessary if the system is affected by unsteady probability density function, so at each time step a new multiresolution representation should be computed without using information from the previous time steps.

Let us consider only the dependence of a scalar function $u = u(\xi)$ from the stochastic space $\Xi = [0, 1]$. The TE strategy is constituted by the following steps (the notation is the same of the Harten's multiresolution framework, i.e $k = 0$ for the finest level and $k = L$ for the coarsest):

- Initialization

  - Fix a threshold ε (the solution is assumed to be solved with this threshold on the finest grid [2]);

  - Fix an index $m_{\max} \in \mathbb{N}$ for the maximum allowed level ($N_{\max} = N_0 = 2^{m_{\max}}$);

  - Fix an index $m_L \in \mathbb{N}$ for the coarsest level ($N_L = 2^{m_L}$);

  - The condition $m_L < m_{\max}$ must be satisfied.

- Evaluation of the function u at each location at the coarsest level $u(\xi_j^L) = u_j^L$ with $j = 0, \ldots, N_L$ where

$$\mathcal{G}^L = \left\{\xi_j^L\right\}_{j=0}^{N_L}, \quad \xi_j^L = jh_L, \quad h_L = 2^L h_0, \quad N_L = N_0/2^L, \tag{4}$$

  and $h_0 = 1/N_0$. Each level can be labeled computing the equivalent index k_{eq}

$$k_{eq} = \log_2\left(\frac{N_0}{N_{k_{eq}}}\right).$$

- Evaluation of the subsequent level, with respect to the coarsest

$$\mathcal{G}^{L-1} = \left\{\xi_j^{L-1}\right\}_{j=0}^{N_{L-1}}, \quad \xi_j^{L-1} = jh_{L-1}, \quad h_{L-1} = 2^{L-1}h_0, \quad N_{L-1} = N_0/2^{L-1}. \tag{5}$$

[2] This is the same hypothesis of the classical MR framework.

- Starting of the adaptive strategy by means of a recursive procedure

  A - The *wavelets coefficients* are computed for the present level k as

  $$d_j^k = u_j^k - \frac{1}{2}\left(u_{\frac{j+1}{2}}^{k+1} + u_{\frac{j-1}{2}}^{k+1}\right) \quad \text{for} \quad 0 \leq j \leq N_k \quad \text{with} \quad j \text{ odd}; \tag{6}$$

  This is one of the occurences where the linear interpolation is used. If more accurate interpolant are used, the detail in (6) will still be the difference betweent the actual value and the value of the interpolant at the interpoation location.

  B - The wavelets coefficients are compared with the threshold $\varepsilon_k = \varepsilon/2^k$. If $|d_j^k| > \varepsilon_k$ then the two nodes ξ_{2j+1}^{k-1} and ξ_{2j-1}^{k-1} will be flagged as active on the next finer mesh $\mathcal{G}^{k-1}$. If $|d_j^k| < \varepsilon_k$ then the *wavelets* is truncated, i.e. its value is posed zero.

  C - The new level $k-1$ is generated if $k > 0$ and only on the activated points the function u is evaluated.

  D - Moving from a level k to the finer adjacent one $k-1$, three different cases are possible:

  * If $\xi_j^k \in \mathcal{G}^k \cap \mathcal{G}^{k+1}$ then $u_j^k = u_{2j}^{k+1}$ (shifting)
  * If $\xi_j^k \notin \mathcal{G}^k \cap \mathcal{G}^{k+1}$ and it is not flagged then interpolate

  $$u_j^k = \frac{1}{2}\left(u_{\frac{j+1}{2}}^{k+1} + u_{\frac{j-1}{2}}^{k+1}\right) \tag{7}$$

  The relation (7) is the second, and last, occurence where the interpolant is used. In case of more accurate interpolant, (7) is replaced by the value of the interpolant on $\mathcal{G}^{k+1}$ at ξ_j^k.

  * If $\xi_j^k \notin \mathcal{G}^k \cap \mathcal{G}^{k+1}$ and it is flagged as active (by the step B of the algorithm) then evaluate, i.e. call the model.

  E - The algorithm stops when the maximum level is reached or when all the *wavelets* coefficients can be truncated (at a certain level $k > 0$).

Some remarks could be done at this point to make things consistent with the application of this strategy to the computation of statistics. For computing a statistics quantity, the following integrals should be computed,

$$\mathcal{E} = \int_{\Xi} u(\xi)p(\xi)\mathrm{d}\xi, \tag{8}$$

where $\mathcal{E}$ is the expectancy of u dependent on the random parameter ξ with pdf $p(\xi)$ in the space Ξ. The TE strategy presented above is applied to the product of $u(\xi)$ and $p(\xi)$. In the general case of unsteady pdf, this procedure must be also applied at each time step and the information between successive time steps must be exchanged by the time advancing technique presented in the next section.

3.2. An accurate preserving time advancing technique

The aim of the TE strategy and the time stepping technique is to minimize the number of points in the space $\Xi \times T$. The unsteady solution should be solved on all the possible trajectories in the space T, then this implicitly involves to know the solution in all the points in $\Xi \times T$. The procedure we propose relies on the application of a multiresolution encoding and truncation of the solution at each time steps. This ensures that the overall error is bounded by (3). Moving from the initial condition toward the ultimate time step can be performed, for each trajectory, by advancing the overall space Ξ time step by time step. This reflects, in the case of an ordinary differential equation, in the computation of the solution $u(\bar{\xi}, \bar{t})$ in a fixed point $\bar{\xi}$ at the time $\bar{t}$ knowing the solution at the previous time steps for all $\xi \in \Xi$ and $t < \bar{t}$. In a rigorous sense, the solution is known only in a limited set of points, *i.e.* the activated points of the TE strategy. However, relying on the result (3), if a point in the portion of the space $\Xi \times T$ with $t < \bar{t}$ is needed, an interpolation can be performed, with the same operator $\mathcal{I}$ employed by the TE strategy, with an error bounded by ε. The final result is to obtain, for each point $\xi \in \Xi$, some trajectories in T where the evaluations could stop and

interpolations could start (from the adjacent ones). Eventually these sequences of interpolations and evaluation can continue to invert virtually at each time step.

A schematic view of these sequences of interpolation and evaluations is reported in figure 1. The points shown are related to the activated points at each time step while the lines indicate the advancing in time that can be performed from a known point (continuous line) or from an interpolated value (dashed lines).

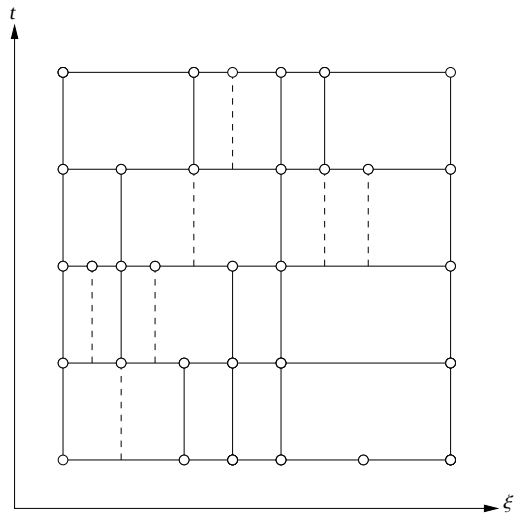

Figure 1: Time advancing. In dashed line the advancing in time from interpolated values and with continuous line the integration from computed value.

3.3. Extension to physical dependent solutions

In this section, we show how the TE strategy, presented in the last two sections, can evolve in the spatial-TE (sTE)strategy, *i.e.* can be extended to partial differential equations. Let us consider partial differential equation defined on 1D physical and stochastic spaces. Obviously, the numerical scheme associated to an adaptive distribution of points in the space $D \times T \times \Xi$, cannot be independent from the specific equation to solve. In this section, the procedure is described in a general way supposing to have a deterministic numerical scheme able to compute the solution $u(\bar{x}, \bar{t}, \bar{\xi})$ knowing all the solutions $u(x, t, \xi)$ for all $x \in D$, $\xi \in \Xi$ and $t < \bar{t}$. In the section §4, an example of the application of the present strategy to the heat equation is illustrated.

The key idea of the algorithm is to fix a finer enough spatial discretization, as well as a time discretization, in order to solve the deterministic problem with the desired accuracy. These requirements are the same of the classical MR approach. In fact, it is clear that the MR scheme cannot produce more accurate solutions than the non compressed finest level solution (remember the estimation (3)). Once the deterministic scheme is provided, the parameters for the TE algorithm, in the stochastic space, must be provided: a maximum level m_{max}, a minimum level m_L and a threshold ε. According to the mathematical setting of the problem, the initial condition must be discretized on the grid $D \times \Xi$ employing the finest resolution level (m_{max}) in the stochastic space and the fixed spatial discretization chosen. Two different cases can arise here: the initial condition is affected by uncertainty or not. However in both cases we can suppose to know analytically the initial condition. After these preliminaries, the spatial-TE (sTE)strategy can be employed as follows. At each time step and for each spatial node, the TE strategy is applied to the associated stochastic space Ξ obtaining the MR representation of the solution $u(\bar{x}, \bar{t}, \xi)$, *i.e.* the representation of the 1D (in this case) stochastic function obtained at a fixed physical space $\bar{x}$ and time $\bar{t}$ location (see figure 2).

Once all the physical points are used by the algorithm, the solution $u(x, \bar{t}, \xi)$ is known. In fact, if a point is evaluated, an *exact* solution is provided for it, otherwise it can be interpolated, employing the operator $\mathcal{I}$ of the TE strategy along the stochastic space with an error bounded by the threshold ε. This procedure continues until the final time step is reached. Obviously, depending on the spatial and time discretization adopted for the problem, different stencils in the physical space could be required. This stencil must be assembled, knowing the solution at

the previous time step, eventually by interpolation along the stochastic space. For instance, in the case of a finite element discretization with a fourth order Runge-Kutta scheme the stencil can be identified in an automatic way using only the finite element mass matrix and stiffness matrix. All the details are reported in the section §4. Once the stencil is reconstructed, the value of the function in all the nodes belonging to the stencil must be computed. Two different situation are possible: the point has been already computed or an interpolation must be performed (with the interpolation operator $\mathcal{I}$ along the stochastic space). We remark that the interpolation must be performed always in the stochastic direction while the stencil assembling procedure could require to use different multiresolution representation at different physical locations (see figure 2).

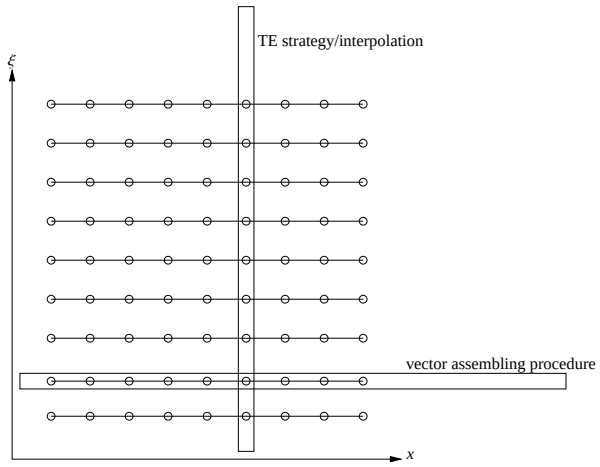

Figure 2: Sketch of the interpolation (same direction of the TE strategy) and stencil assembling procedures.

The entire sTE strategy can be summarized as follows :

- Preliminary
  - Choose a deterministic solver with a spatial fixed discretization and a proper time discretization technique;
  - Fix the parameters for the TE strategy: finest level m_{max}, coarsest level m_L and threshold ε;

- sTE
  - For each time step and for each spatial node, the TE strategy should be applied in order to represent the solution along the stochastic space;
  - The proper stencil must be assembled using different spatial locations (see figure 2); some interpolations along the stochastic space could be necessary at this stage.

In the next section, this algorithm will be adapted to the heat equation discretized by a finite element method in the physical space and a fourth order Runge-Kutta method in time.

4. A Finite Elements deterministic solver

In this section, we present the discretization of the heat equation, described by a parabolic partial differential equation with a random initial condition.

Let us describe the equations for the homogeneous 1D case ($x \in D = [0,1]$) and temporal domain $t \in T = [0, t_f]$:

$$\begin{cases} \dfrac{\partial u(x,t,\xi)}{\partial t} = \nu \dfrac{\partial^2 u(x,t,\xi)}{\partial x^2}, & \xi \in \Xi \\ u(0,t,\xi) = u(1,t,\xi) = 0, & \text{for} \quad t \in T \\ u(x,0,\xi) = u_0(x,\xi), \end{cases} \tag{9}$$

where the initial conditions is supposed uncertain.

The problem (9) can be recast in the weak form multiplying both side for a test function $v \in V = H_0^1(0,1)$, *i.e.* the space $H^1(0,1)$ with null elements at the boundary of the domain, and then integrating over the physical space $D = [0,1]$:

$$\int_D \frac{\partial u(x,t,\xi)}{\partial t} v \, \mathrm{d}x + \int_D \nu \frac{\partial u(x,t,\xi)}{\partial x} \frac{\partial v}{\partial x} \, \mathrm{d}x = 0. \tag{10}$$

The Galerkin formulation of the problem can be obtained searching the (approximated) solution in the finite dimensional space: $u_h = \sum_{i=1}^{N_h} u_i(t;\xi)\phi_i(x) \in V_h$. The space V_h is the so-called finite element space of basis $\{\phi_j\}_{j=1}^{N_h}$.

After some manipulations (for more details see Appendix A), the following algebraic problem is obtained :

$$\mathrm{M}\frac{\mathrm{d}\mathbf{U}(t)}{\mathrm{d}t} = -\nu \mathrm{A}\mathbf{U}, \tag{11}$$

where the so-called mass M and stiffness A matrices are of $(N_h \times N_h)$ dimension and the vector $\mathbf{U}$ is employed to collect all the degree of freedom of the problem $\mathbf{U}(\mathbf{t}) = \{u_1(t), u_2(t), \ldots, u_{N_h}(t)\}^{\mathrm{T}}$. We remark here that the present formulation is quite general not depending on the number of physical space dimensions. As reported in Appendix A, the matrices M and K are quite sparse and symmetric. In particular, if the finite element space of linear functions is employed, the matrices are both tridiagonal.

Finally, the initial parabolic partial differential system of equations, is reduced to a system of ordinary differential equations (ODEs). In the next section, the time integration technique is illustrated.

4.1. A recast fourth-order Runge-Kutta

In this section, we aim to use a time integration technique permitting to apply the sTE strategy in order to solve the stochastic partial differential problem (9). The TE technique, described in Section 3, requires the solution of the problem in a specific point of the space $(\bar{x}, \bar{t}, \bar{\xi})$, whenever all the solution at the previous time steps $t < \bar{t}$ are available. This means that the numerical scheme adopted to solve the system of ODEs should be able to compute the solution in a certain node $\bar{i}$ at the time $\bar{t}$ knowing the solution in all the nodes at time $t < \bar{t}$. As it has been described in §3, the TE strategy is employed in the stochastic direction, while, obviously, the deterministic solver produces solutions in the physical space. The coupling between these two spaces will be described more in details in Section §4.3.

For instance, let us suppose to know the solution $\mathbf{U}(\mathbf{t})$ for $t < \bar{t}$ and that the deterministic solver is able to compute the $\bar{i}$-th coefficient of the vector $\mathbf{U}(\bar{\mathbf{t}})$, *i.e.* the $\bar{i}$-th degree of freedom of the finite element expansion of the solution $u_h \in V_h$. In this work, we choose to use an explicit time integration technique, in particular the fourth order Runge-Kutta scheme [18], described as follows for a Cauchy problem :

$$\begin{cases} \dot{y}(t) &= f(t, y(t)) \quad t \in [0, t_f] \\ y(0) &= y_0, \end{cases} \tag{12}$$

where $y \in C(0, t_f)$ can be formulated as [18]

$$y_{n+1} = y_n + \frac{\Delta t}{6}\left(k_1 + 2k_2 + 2k_3 + k_4\right), \tag{13}$$

where $y_n = y(t_n)$ with $t_n = n\Delta t$ and

$$\begin{cases} k_1 = f(t_n, y_n) \\ k_2 = f\left(t_n + \dfrac{\Delta t}{2}, y_n + \dfrac{\Delta t}{2} k_1\right) \\ k_3 = f\left(t_n + \dfrac{\Delta t}{2}, y_n + \dfrac{\Delta t}{2} k_2\right) \\ k_4 = f\left(t_n + \Delta t, y_n + \Delta t k_3\right) : \end{cases} \tag{14}$$

In this form, the Runge-Kutta (RK4) method is extended to a system of ODEs in a straightforward manner.

In the case of the heat equation, the system of ODEs (11) can be recast to a set of decoupled equations if the so-called *mass lumping* technique is adopted. In particular, as shown in Appendix A, if a trapezoidal integration

technique is employed to compute the term of the mass matrix M, a diagonal matrix can be obtained and, in the case of linear element, each term of the mass matrix can be computed as the summation by rows of the elements

$$\hat{m}_{ii} = \sum_{i=1}^{N_h} m_{ij}, \tag{15}$$

where m_{ij} indicates the generic element of the mass matrix M at the $i-$th row and $j-$th column.

If we indicate with $\hat{\mathrm{M}}$ the corresponding lumped mass matrix, the system of ODEs can be written as

$$\frac{\mathrm{d}\mathbf{U}(t)}{\mathrm{d}t} = -\nu\hat{\mathrm{M}}^{-1}\mathrm{A}\mathbf{U}(\mathbf{t}) = \mathbf{f}(\mathbf{U}(\mathbf{t})) \tag{16}$$

and the corresponding RK4 scheme is

$$\begin{cases} \mathbf{U}_{n+1} = \mathbf{U}_n + \dfrac{\Delta t}{6}\left(\mathbf{k_1} + 2\mathbf{k_2} + 2\mathbf{k_3} + \mathbf{k_4}\right) \\ \mathbf{k_1} = -\nu\hat{\mathrm{M}}^{-1}\mathrm{A}\mathbf{U}_n \\ \mathbf{k_2} = -\nu\hat{\mathrm{M}}^{-1}\mathrm{A}\left(\mathbf{U}_n - \nu\hat{\mathrm{M}}^{-1}\mathrm{A}\mathbf{U}_n\right) = \mathbf{k_1} + \nu^2\dfrac{\Delta t}{2}\left(\hat{\mathrm{M}}^{-1}\mathrm{A}\right)^2\mathbf{U}_n \\ \mathbf{k_3} = -\nu\hat{\mathrm{M}}^{-1}\mathrm{A}\left(\mathbf{U}_n + \dfrac{\Delta t}{2}\mathbf{k_1} + \nu^2\dfrac{\Delta t^2}{4}\left(\hat{\mathrm{M}}^{-1}\mathrm{A}\right)^2\mathbf{U}_n\right) = \mathbf{k_2} - \nu^3\dfrac{\Delta t^2}{4}\left(\hat{\mathrm{M}}^{-1}\mathrm{A}\right)^3\mathbf{U}_n \\ \mathbf{k_4} = -\nu\hat{\mathrm{M}}^{-1}\mathrm{A}\left(\mathbf{U}_n + \Delta t\,\mathbf{k_1} + \nu^2\dfrac{\Delta t^2}{2}\left(\hat{\mathrm{M}}^{-1}\mathrm{A}\right)^2\mathbf{U}_n - \nu^3\dfrac{\Delta t^3}{4}\left(\hat{\mathrm{M}}^{-1}\mathrm{A}\right)^3\mathbf{U}_n\right) \\ \qquad = \mathbf{k_1} + \nu^2\Delta t\left(\hat{\mathrm{M}}^{-1}\mathrm{A}\right)^2\mathbf{U}_n - \nu^3\dfrac{\Delta t^2}{2}\left(\hat{\mathrm{M}}^{-1}\mathrm{A}\right)^3\mathbf{U}_n + \nu^4\dfrac{\Delta t^3}{4}\left(\hat{\mathrm{M}}^{-1}\mathrm{A}\right)^4\mathbf{U}_n \end{cases} \tag{17}$$

To compute the $\bar{i}-$th term of the vector $\mathbf{U}(t_{n+1})$ is then necessary to compute the corresponding term $\bar{i}-$th term of each vector $\mathbf{k_1}$, $\mathbf{k_2}$, $\mathbf{k_3}$ and $\mathbf{k_4}$. This can be done efficiently if four matrices are stored at the beginning of the computation $\left(\hat{\mathrm{M}}^{-1}\mathrm{A}\right)$, $\left(\hat{\mathrm{M}}^{-1}\mathrm{A}\right)^2$, $\left(\hat{\mathrm{M}}^{-1}\mathrm{A}\right)^3$, $\left(\hat{\mathrm{M}}^{-1}\mathrm{A}\right)^4$. We remark that $\hat{\mathrm{M}}^{-1}$ indicates the inversion of a diagonal matrix and then the product $\hat{\mathrm{M}}^{-1}\mathrm{A}$ can be done in a very non expensive way. Once the four matrices are computed, the $\bar{i}-$th term of the four vectors $\mathbf{k_1}$, $\mathbf{k_2}$, $\mathbf{k_3}$ and $\mathbf{k_4}$, can be computed (less than a multiplying factor), as the scalar product between the $\bar{i}-$th row vector (of each of the four $\mathbf{k_1}$, $\mathbf{k_2}$, $\mathbf{k_3}$ and $\mathbf{k_4}$ matrices) and the vector $\mathbf{U}_n$ (already known from the stencil assembling procedure). This procedure allows to select automatically the stencil needed by the time integration technique. For adapting this deterministic scheme to the solution of the stochastic parabolic equation by the sTE strategy, the reconstruction of the vector $\mathbf{U}_n$ from the different multiresolution representation (one for each physical node) of the solution is needed; this will be described in detail in section 4.3.

Obviously, if the deterministic scheme described above is applied for each time step to each node of the physical grid, the time dependent solution of the problem on the whole physical space $x \in D = [0, 1]$ can be computed when a fixed value for the parameter $\xi \in \Xi = [0.2, 0.8]$ is chosen. The sTe strategy, as shown in §3, needs to fix a physical mesh on which the deterministic solution can be represented with the desired accuracy. To identify the proper mesh to employ in the section §5, a spatial convergence study is reported in the next section.

4.2. Space convergence for the deterministic solver

In this section, the space convergence properties of the deterministic scheme is presented. For this reason, a reference solution should be computed. Then, the equivalent modal problem using the method originally proposed by Fourier is solved.

The solution can be searched as a product of two functions depending only from the space and time, respectively. This technique, called separation of variable, with $u(x, t) = f(x)g(t)$, leads to

$$\frac{1}{g(t)}\frac{\mathrm{d}g(t)}{\mathrm{d}t} = \nu\frac{1}{f(x)}\frac{\mathrm{d}^2 f(x)}{\mathrm{d}x^2} = -\lambda, \tag{18}$$

where λ must be a constant value not depending neither by x or t. Non trivial solution exist only if $\lambda > 0$ as

$$\begin{cases} f(x) = A\sin(\sqrt{\lambda}x) + B\cos(\sqrt{\lambda}x) \\ g(t) = Ce^{-\nu\lambda t}. \end{cases} \tag{19}$$

The application of the boundary condition to the spatial function $f(x)$ makes possible to compute $B = 0$ and $\lambda = n^2\pi^2$ where the integer n indicates the $n-$th mode of the function $f(x)$:

$$f(x) = \sum_{n=1}^{\infty} A_n \sin(n\pi x). \tag{20}$$

The solution $u(x,t)$ is the product of the two functions ($f(x)$ and $g(t)$) and it becomes

$$u(x,t) = C\sum_{n=1}^{\infty} A_n \sin(n\pi x)e^{-\nu\lambda t} = \sum_{n=1}^{\infty} H_n \sin(n\pi x)e^{-\nu\lambda t} = \sum_{n=1}^{\infty} H_n \Psi_n(x) \tag{21}$$

The amplitude H_n for each mode can be obtained by normalization employing the orthogonality between modes, *i.e.* $\int_0^1 \Psi_i\Psi_j \mathrm{d}x = H_n\delta_{ij}$ where δ_{ij} is the Kronecker delta function, and the initial condition $u_0(x)$

$$H_n \int_0^1 \sin(n\pi x)\sin(n\pi x)\mathrm{d}x = \frac{1}{2}H_n = \int_0^1 u_0(x)\sin(n\pi x)\mathrm{d}x \longrightarrow H_n = 2\int_0^1 u_0(x)\sin(n\pi x)\mathrm{d}x. \tag{22}$$

The modal truncated solution with a large number of modes $N_{mod} = 10\,000$ with each term H_n computed by a trapezoidal rule on an equally spaced mesh of 100 000 points has been employed as reference solution. In the figure 3, different solutions computed on uniform meshes of 51, 101 and 201 points are reported in 3(a), while the errors measured in norm L_2 are shown in 3(b) for the same meshes.

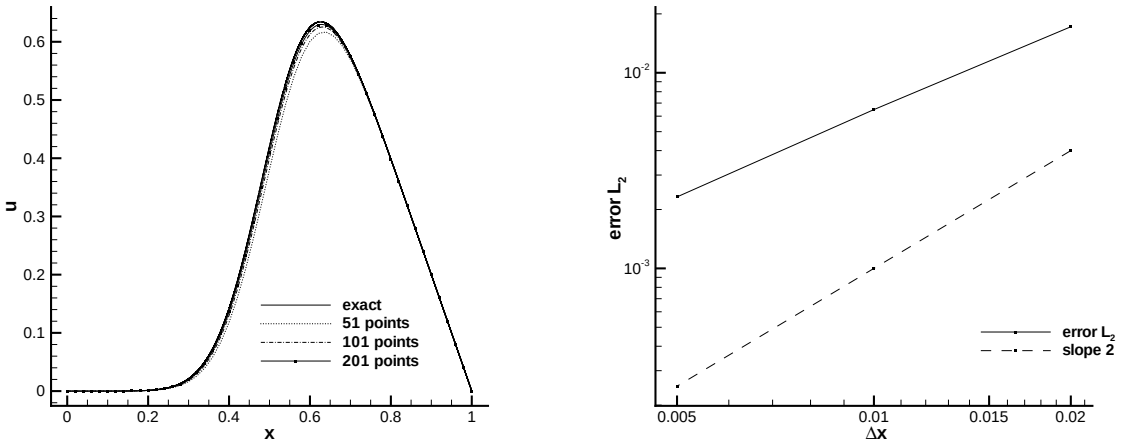

(a) (b)

Figure 3: Space convergence for the FE deterministic solver. (a) Solutions with different spatial resolutions and (b) L_2 error norm of the solution with respect the reference modal solution ($\nu = 0.01$ and $a = 1$).

As it can be observed from these results, the mesh with 101 points shows to be finer enough to achieve a good spatial accuracy and then it will be adopted for the computations. For stability and accuracy requirements, a time step equal to $\Delta t = 0.001$ (the same employed in the spatial convergence results) is a good trade-off.

The coupling between the deterministic scheme and the TE strategy described in section 3 is described with more detail in the next section.

4.3. sTE strategy applied to the 1D heat equation

In this section, the algorithm for the stochastic heat equation is presented. The deterministic solver employs a spatial finite element discretization and a Runge-Kutta method to integrate the solution in time. The scheme is able to compute a specific degree-of-freedom $u_{\bar{i}}(t_{n+1})$ when the vector of all the degree-of-freedom $\mathbf{U}(t_n)$ at the previous time step is provided. This is not dependent on the finite element space, *i.e.* the degree of the basis functions. A sequence of evaluations must be performed for all the activated points (in the TE strategy) at different locations in the physical and stochastic space. However, the vector $\mathbf{U}(t_n)$ could not be available for each parameter ξ (see figure 2). This issue is solved in the sTE strategy performing an interpolation, along the stochastic space, in order to compute the value at a certain physical location by means of the stencil assembling procedure.

The complete algorithm for the sTE strategy applied to the heat equation (9) is as follows :

- Preliminary
  - A fixed uniform spatial resolution is fixed with points: $\{x_i\}_{i=0}^{N+1}$;
  - A uniform time discretization is chosen $t_n = n\Delta t$, where $\Delta t = t_f/N_t$ with N_t number of time steps;
  - The parameters for the TE strategy are fixed: m_L, m_{max} and ε;
  - The mass matrix M is computed, lumped and inversed obtaining $\hat{\mathrm{M}}^{-1}$;
  - The stiffness matrix A is computed;
  - The four matrices $(\hat{\mathrm{M}}^{-1}\mathrm{A})$, $(\hat{\mathrm{M}}^{-1}\mathrm{A})^2$, $(\hat{\mathrm{M}}^{-1}\mathrm{A})^3$, $(\hat{\mathrm{M}}^{-1}\mathrm{A})^4$ are computed and stored.
- sTE strategy
  - For each time step all the (internal) spatial nodes $\{x_i\}_{i=1}^{N}$ are considered;
  - For each spatial node $x_{\bar{i}}$ considered, a MR representation is obtained for $u(x_{\bar{i}}, t_{n+1}, \xi)$ in the stochastic space;
    - A- To evaluate the solution in $(x_{\bar{i}}, t_{n+1}, \xi_{\bar{j}})$, the vector $\mathbf{U}(t_n, \xi_j)$ must be assembled;
    - B- $k_{1\bar{i}}$, $k_{2\bar{i}}$, $k_{3\bar{i}}$, $k_{4\bar{i}}$ are computed employing the $\bar{i}$–th row of the four matrices $(\hat{\mathrm{M}}^{-1}\mathrm{A})^n$ and $\mathbf{U}(t_n, \xi_j)$;
    - C- Evaluation: $u(x_{\bar{i}}, t_{n+1}, \xi_{\bar{j}}) = U_{\bar{i}}(t_n, \xi_{\bar{j}}) + \dfrac{\Delta t}{6}(k_{1\bar{i}} + 2k_{2\bar{i}} + 2k_{3\bar{i}} + k_{4\bar{i}})$.

The vector assembling procedure for the vector $\mathbf{U}(t_n, \xi_{\bar{j}})$, is illustrated in the case of linear interpolation as follows:

- For all the nodes $\{x_i\}_{i=1}^{N}$, if the point $(x_i, t_n, \xi_{\bar{j}})$ has been already computed, the value is stored in $U_i(t_n, \xi_{\bar{j}})$;
- Otherwise the left and right values are identified for interpolation as follows:
  - Left value: greater value of ξ_j at the i–th spatial position less than $\xi_{\bar{j}}$;
  - Right value: point ξ_{j+1} at the i–th spatial position;
  - Interpolation: linear interpolation between ξ_j and ξ_{j+1} at the stochastic position $\xi_{\bar{j}}$.

The procedure described in this section is able to reduce the overall number of evaluations in the space $D \times T \times \Xi$ by determining the important point, *i.e.* the points that cannot be interpolated within the prescribed error with the chosen interpolation operator. The final result is an unsteady pattern of the activated points in the space $D \times \Xi$ on which the solution is computed by means of the deterministic solver, while the remaining point are interpolated.

5. Numerical results

In this section, the sTE strategy is applied to some numerical problems: a steady discontinuous function (§5.1); an ordinary differential equation (§5.2) with the application of the time integration strategy reported in §3.2. Finally, the stochastic partial differential equation (9) describing the heat conduction and the evolving temperature u along a 1D rod subjected to an uncertain and discontinuous initial condition, is solved by means of the sTE strategy in (§5.3).

In this section, the expectancy $\mathcal{E}$ and the variance Var for a generic function $f(\xi)$, are computed according to the following definitions

$$\begin{aligned} \mathcal{E}(f(\xi)) &= \int_{\Xi} f(\xi)p(\xi)\mathrm{d}\xi \\ \mathrm{Var}(f(\xi)) &= \int_{\Xi} (f(\xi) - \mathcal{E}(f(\xi)))^2 p(\xi)\mathrm{d}\xi, \end{aligned} \tag{23}$$

where the probability distribution $p(\xi)$ is chosen systematically as uniform.

All the results reported in this section are compared to two classical methods in uncertainty quantification, namely Monte Carlo (MC) and Polynomial Chaos (PC). These two methods are employed in a complete non-intrusive way and the reference solution is assumed to be the fully converged Monte Carlo solution.

5.1. Steady problem

The first example is a function $f(\xi) : \Xi \rightarrow \mathbb{R}$ where ξ is a random parameter having an uniform distribution $\xi \sim \mathcal{U}[0,1]$. Function f_3 is a piecewise function, composed by a tangent and a wave sine function with decreasing wavelength (see figure 4(a)):

$$f_3(\xi) = \begin{cases} \tan(\xi\pi) & \xi \leq 0.41234 \\ \sin(5\pi\xi^4) & \xi > 0.41234 \end{cases} \tag{24}$$

The coarsest level is assumed to be equal to 2^1 ($m_l = 1$) intervals, while the finest one to 2^8 ($m_{max} = 8$). The threshold is fixed to $\varepsilon = 10^{-1}$ with a variation related to the refinement level (k) equal to $\varepsilon_k = \varepsilon/2^k$. In figure 4(b), the sequence of evaluated points (N_{eval}) is reported. The circles represent the evaluations of the function $f(\xi)$, while a full black dots indicate the activated, i.e. greater than the threshold ε_k, *wavelets* N_w. It is evident that the algorithm is capable to follow the discontinuity and to add some points where needed, *i.e.* in regions with high gradients in the stochastic space.

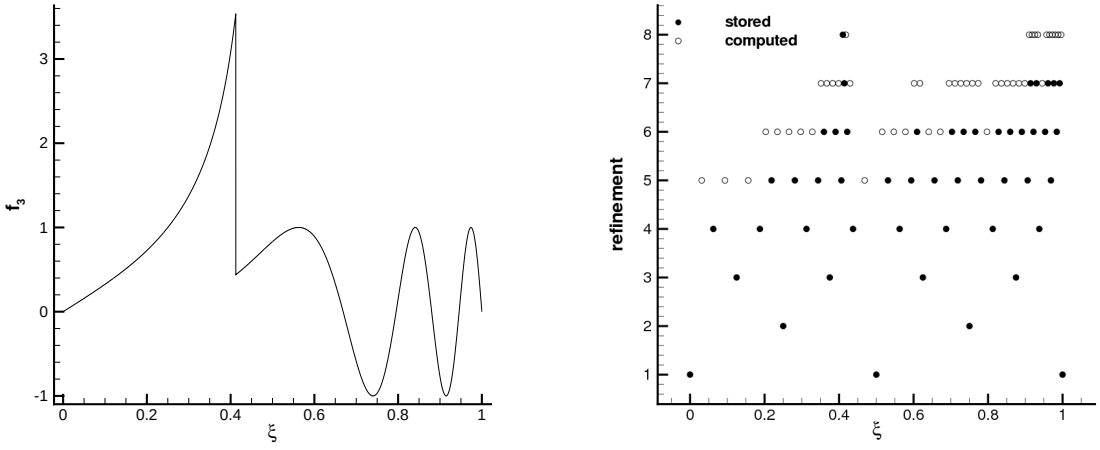

(a) (b)

Figure 4: Function $f_3(\xi)$ (a) and the pattern of computed and activated (stored) points (b).

In the table 1, the compression properties of the sTE strategy are reported when applied to the function f_3. In particular, the compression μ_{cr} and the evaluation τ ratios reported in the table 1 are computed as follows

$$\begin{aligned} \mu_{cr} &= \frac{2^{m_{max}} + 1}{N_w + 2^{m_L} + 1} \\ \tau &= \frac{2^{m_{max}} + 1}{N_{eval}}. \end{aligned} \tag{25}$$

They indicate the ratio between the number of points of the non-compressed solution and the number of activated wavelets (these sets include the points of the coarsest level) and the ratio between the number of points at the finest level and the number of evaluations N_{eval} needed by the TE strategy, respectively.

The error norms reported in the table 1 are computed in the L_1 and L_∞ space as

$$\begin{aligned} \mathrm{err}_{L_1} &= \|f^0 - \hat{f}\|_{L_1} = \frac{1}{N}|f_i^0 - \hat{f}_i| \\ \mathrm{err}_{L_\infty} &= \|f^0 - \hat{f}\|_{L_\infty} = \max_i |f_i^0 - \hat{f}_i|, \end{aligned} \tag{26}$$

where f^0 is the function at the finest level and $\hat{f}$ is the compressed function, i.e. the function evaluated only in the set of points corresponding to the activated wavelets.

m_{max}	N_{sto}	N_{eval}	μ	τ	err L_1	err L_∞
5	21	29	1.571429	1.137931	0.1341053E-01	0.7356531E-03
6	31	49	2.096774	1.326531	0.1160966E-01	0.8490046E-03
7	39	73	3.307692	1.767123	0.1003391E-01	0.1228993E-02
8	49	95	5.244898	2.705263	0.1291483E-01	0.1506392E-02
9	58	113	8.844828	4.539823	0.8991428E-02	0.1307482E-02

Table 1: Final result for the function f_3 ($\varepsilon = 10^{-1}$)

Thanks to the adaptive distribution of points, the present strategy allows computing the statistical moments very efficiently even with a simple quadrature formula (like the composite trapezoidal rule [18]). This is not the case for MC or PC methods.

The percentage errors with respect the reference MC solution with 2×10^6 deterministic runs is computed as follows

$$\begin{aligned} \mathrm{err}_{\mathcal{E}} &= \frac{|\mathcal{E} - \mathcal{E}_{\mathrm{exact}}|}{\mathcal{E}_{\mathrm{exact}}} 100 \\ \mathrm{err}_{Var} &= \frac{|Var - Var_{\mathrm{exact}}|}{Var_{\mathrm{exact}}} 100. \end{aligned} \tag{27}$$

They are reported in figure 5 both for mean and variance. The number of points for the PC method are $N = n_0 + 1$, where n_0 is the total degree of the polynomial representation. Concerning the proposed algorithm, several solutions are obtained by varying the maximal level allowed between 2^2 and 2^9 with the coarsest level equal to 2^1 and the threshold $\varepsilon = 10^{-1}$.

The adaptive strategy displays better results both in terms of accuracy and efficiency with respect to the MC and PC methods. For MC and PC, an high non smooth behavior arises when increasing the number of point. This is due to the presence of discontinuities that can prevent the convergence of these quadrature techniques.

5.2. A Differential ordinary equation (0D-1D)

In this section, the case of an ordinary differential equation is addressed. In the following, this case is indicated as 0D in the physical space and 1D in the stochastic space, because there is only one uncertainty affecting the solution of the problem. An ordinary differential problem, extracted from [16], has been modified as follows

$$\begin{cases} \frac{\mathrm{d}\rho}{\mathrm{d}t} = \alpha(\bar{\rho} - \rho) - \gamma\rho - \beta(\rho - \bar{\rho})\rho^2 \\ \bar{\rho} = 1 + \frac{1}{2}\sin(5\omega + 8/5) \\ \beta = 20\omega, \end{cases} \tag{28}$$

where $\alpha = 1$, $\gamma = 0.01$ and $\omega \in \mathcal{U}[0, 1]$. A discontinuous initial solution in the stochastic space is chosen in order to address a more challenging problem with respect to the one proposed in [16] :

$$\rho(t = 0) = \begin{cases} 3/4 \ \text{ if } \ 0.3 < \omega < 0.7 \\ 0 \quad \text{otherwise.} \end{cases} \tag{29}$$

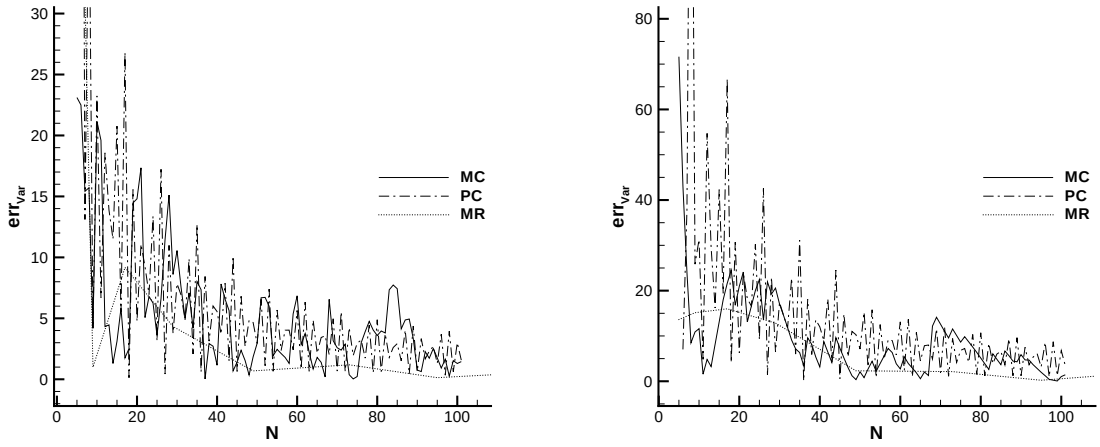

(a) (b)

Figure 5: Percentage error with respect the reference MC solution for the mean (a) and the variance (b).

The time integration is performed by means of an explicit Runge-Kutta scheme, the so-called RK4, with a time step $\Delta t = 0.01$. The multiresolution representation at each time step allows advancing the solution in time along patches constituted by true evaluations and interpolations thanks to the accuracy reconstruction embedded in the multiresolution framework. The final results is a refine/derefine capability in the time-stochastic domain that suits very well the efficiency requirement needed in complex and high costly applications. In the figure 6, the pattern in the space $t - \omega$ of the computed, i.e. evaluated points, is reported.

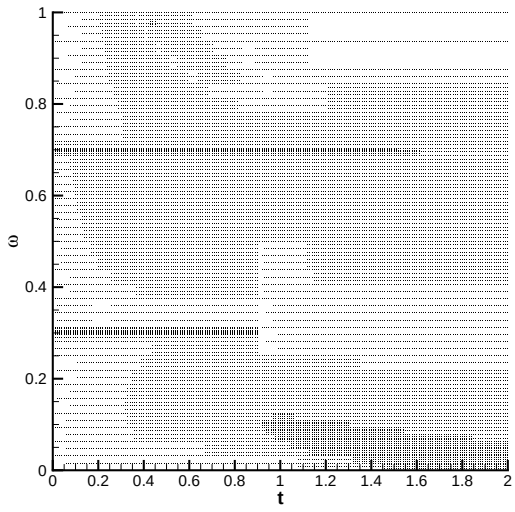

Figure 6: Pattern in the $t - \omega$ space of the computed points of equation 29.

The error of the statistical moments, are reported in figure 7 with respect to a MC reference solution of 2×10^6 points at each time step ($N = 400 \times 10^6$ evaluations in the $\omega - t$ space). Dealing with an unsteady solution, a L_1 norm

(in time) is employed according to the following definitions

$$\begin{aligned} \mathrm{err}_{\mathcal{E}}|_{L_1} &= \|\mathcal{E}(\rho) - \mathcal{E}(\hat{\rho})\|_{L_1} = \frac{1}{N_t}\sum_{i=1}^{N_t}\left|\frac{\mathcal{E}_i(\rho) - \mathcal{E}_i(\hat{\rho})}{\mathcal{E}_i(\hat{\rho})}\right|, \\ \mathrm{err}_{\mathrm{Var}}|_{L_1} &= \|\mathrm{Var}(\rho) - \mathrm{Var}(\hat{\rho})\|_{L_1} = \frac{1}{N_t}\sum_{i=1}^{N_t}\left|\frac{\mathrm{Var}_i(\rho) - \mathrm{Var}_i(\hat{\rho})}{\mathrm{Var}_i(\hat{\rho})}\right|, \end{aligned}$$

where $\mathrm{err}_{\mathcal{E}}$ and $\mathrm{err}_{\mathrm{Var}}$ are the errors for the expectancy and the variance. The solution ρ is compared to the reference solution $\hat{\rho}$ discretized with the same total number of time steps equal to $N_t = \Delta t \times t_f$, where the total time of the simulation t_f is assumed equal to two.

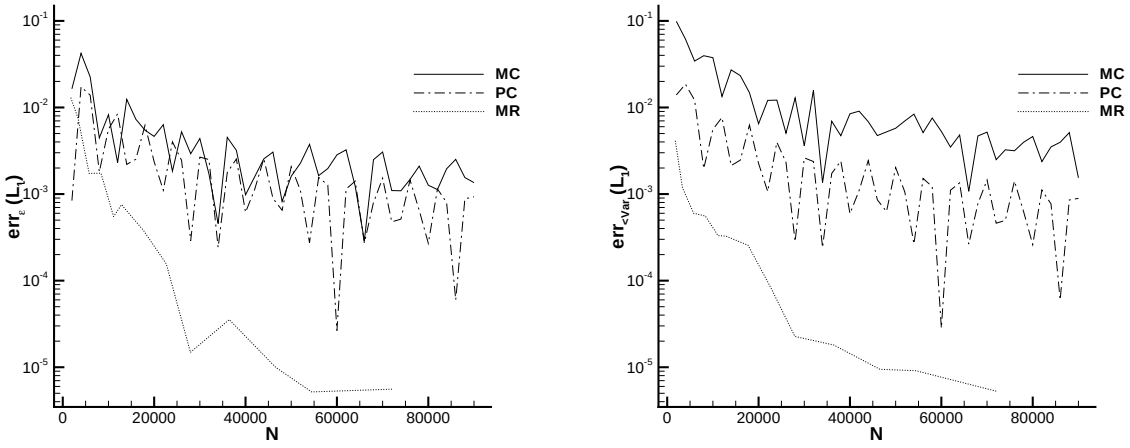

(a) (b)

Figure 7: L_1 norm of the errors for the mean and variance of $\rho(t)$.

The strategy presented in this work exhibits the fastest convergence and a smoother behavior with respect to Monte Carlo and the Polynomial Chaos both for mean and variance. Similar results are obtained for different norms (L_2, L_∞) not reported here for brevity.

5.3. A Partial differential equation (1D-1D)

In this section, the solution of the stochastic parabolic partial differential equation described in (9) is addressed. This unsteady problem is 1D in the physical space and 1D in the stochastic space.

The diffusivity is assumed to be equal to $\nu = 0.01$ and the parameter of amplitude related to the initial condition (30) to $a = 1$.

Let us consider a discontinuous initial condition as follows

$$u_0(x,\xi) = \begin{cases} 0 & \text{if} \quad x < \xi \\ \dfrac{a}{\xi - 1}(x-1) & \text{if} \quad x \geq \xi, \end{cases} \tag{30}$$

with the stochastic parameter $\xi \in \Xi = [0.2, 0.8]$ with uniform distribution in Ξ.

For instance, the initial condition for the parameter $\xi = 0.5$ is reported in figure 8 (for $a = 1$). Relying on the convergence study reported in section 4.2, let us consider a physical domain defined in $D = [0, 1]$ discretized by an uniform mesh of $N_x = 101$ nodes and a uniform time step equal to $\Delta t = 0.001$ for a total time of simulation equal to $t_f = 0.5$ ($N_t = 500$ time steps).

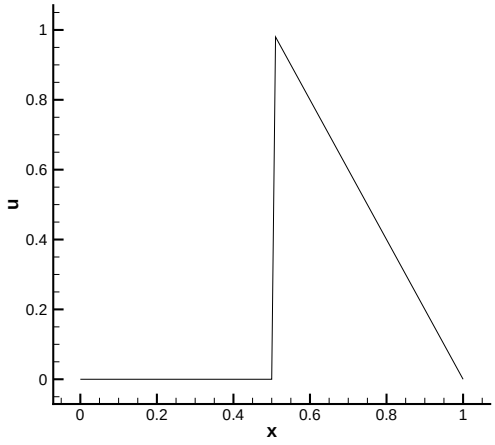

Figure 8: Initial condition for the problem (9) with the stochastic parameter $\xi = 0.5$ on a mesh with 101 equally spaced points.

Concerning the sTE strategy, the initial condition should be discretized on the finest mesh ($N_x \times (2^{m_{max}} + 1)$) in the space $x - \xi$. The initial condition 9(a) of the problem and the meshes corresponding to the solution at time $t = 0.001$ 9(b), $t = 0.25$ 10(a) and $t = 0.5$ 10(b) are reported for the parameters $m_L = 3$, $m_{max} = 11$ and $\varepsilon = 10^{-1}$.

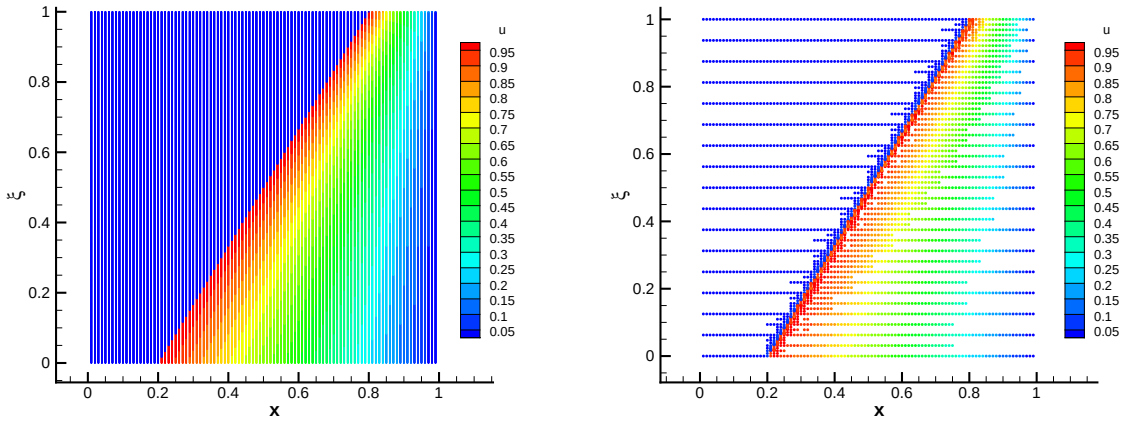

(a) (b)

Figure 9: Meshes corresponding to the initial condition (a) of the problem (9) and the derefined mesh after the first time step (b).

For performing more accurate comparison, a signal is extracted at fixed space locations. Three different probes at the spatial locations $x = 0.2$ (P1), $x = 0.5$ (P2) and $x = 0.8$ (P3) are considered. For each one of these probes, the mean and variance are stored as functions of the time. The error norms (in time) for the L_1 and L_2 spaces are computed as follows

$$\mathrm{err}_{\mu^m}\Big|_{L_p} = \|\mu^m(u,\,t) - \mu^m(\bar{u},\,t)\|_{L_p} = \left(\frac{1}{N_t}\sum_{i=1}^{N_t}\left|\frac{\mu_i^m(u,\,t) - \mu_i^m(\bar{u},\,t)}{\mu_i^m(\bar{u},\,t)}\right|^p\right)^{1/p}, \tag{31}$$

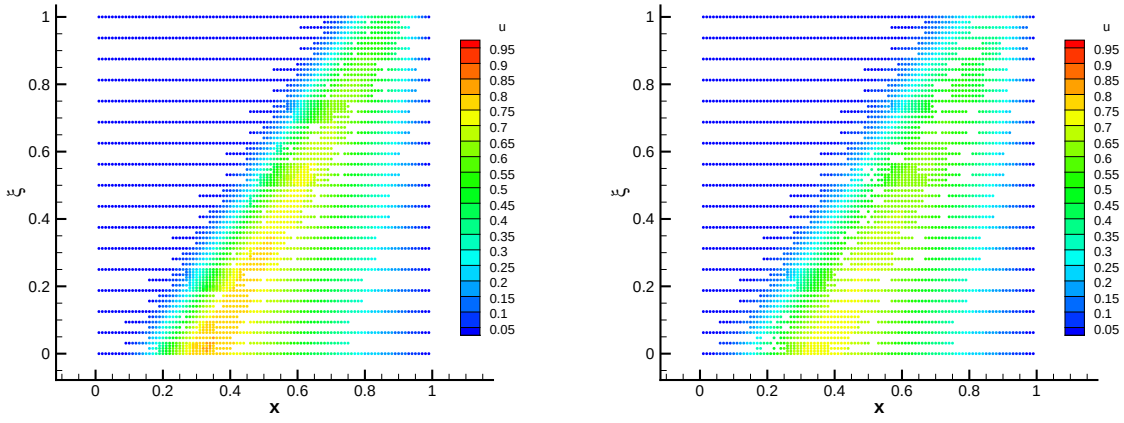

(a) (b)

Figure 10: Meshes corresponding to the half time ($t = 0.25$) simulation (a) and the final time ($t = 0.5$) pattern (b).

while for the L_∞ space

$$\text{err}_{\mu^m}\Big|_{L_\infty} = \|\mu^m(u,\,t) - \mu^m(\bar{u},\,t)\|_{L_\infty} = \max_i \left| \frac{\mu_i^m(u,\,t) - \mu_i^m(\bar{u},\,t)}{\mu_i^m(\bar{u},\,t)} \right|, \tag{32}$$

where the reference solution is indicated as $\bar{u}$ and μ^m indicates both mean and variance. The reference solution is obtained in this case with a fully converged MC solution with the same spatial grid ($N_x = 101$), the same time discretization ($\Delta t = 0.001$) but a number of points in the stochastic space equal to $N_\xi = 2.5 \times 10^6$.

The results for mean corresponding to the three probes are reported in the figures 11, 12 and 13, respectively. The sTE strategy is applied with $m_L = 6$, m_{max} between 8 and 16 with a threshold equal to $\varepsilon = 10^{-1}$. MC and PC results obtained on the same physical mesh and with the same time discretization are also reported. In particular, the two methods are employed with a number of points, in the stochastic space, varying between $N_\xi = 100$ and $N_\xi = 300$ for MC and degree between 100 and 300 for PC. In all the presented results, the number of points N represent the overall number of point of the grid in $D \times T \times \Xi$ equal to $N = N_x \times N_t \times N_\xi$.

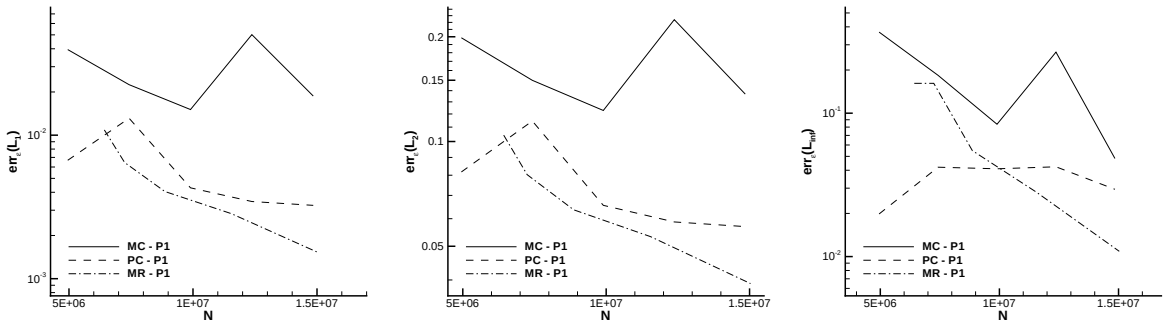

(a) (b) (c)

Figure 11: Error norms of the mean of the variable u, corresponding to the probe P1, for the 1D heat equation problem with uniform pdf in the L_1 (a), L_2 (b) and L_∞ (c) spaces.

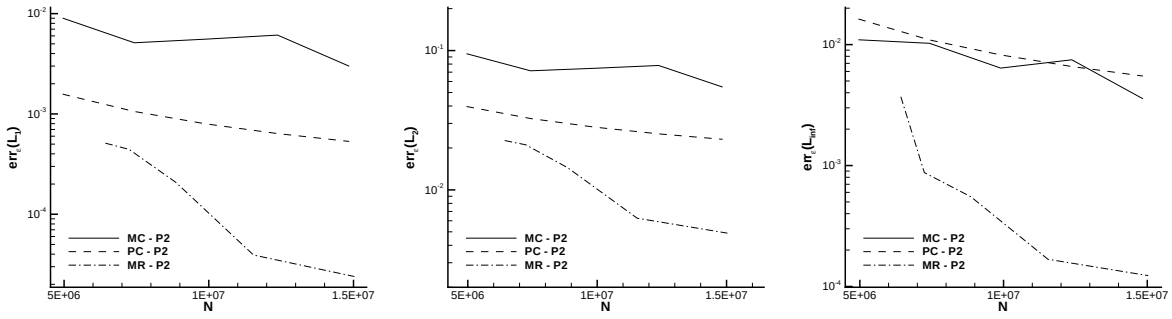

(a) (b) (c)

Figure 12: Error norms of the mean of the variable u, corresponding to the probe P2, for the 1D heat equation problem with uniform pdf in the L_1 (a), L_2 (b) and L_∞ (c) spaces.

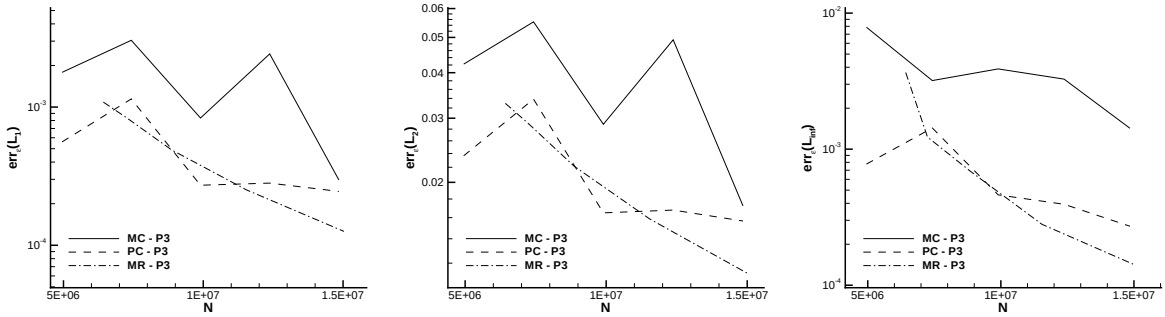

(a) (b) (c)

Figure 13: Error norms of the mean of the variable u, corresponding to the probe P3, for the 1D heat equation problem with uniform pdf in the L_1 (a), L_2 (b) and L_∞ (c) spaces.

All the results display systematically very good performances of the presented approach both in term of accuracy and efficiency. The sTE strategy converges smoothly (and in a monotone way) to higher accurate solutions when a large number of points is considered. This is not the case for MC and PC.

The results concerning the variance for the probes P1, P2 and P3 are reported in figures 14, 15 and 16, respectively.

Except for the variance computed at the probe P2, the behaviour of the proposed approach is monotone and smoother than both MC and PC. A lower error with a lower global number of points is attained by the sTe strategy with respect to MC and PC. The worse behavior of MC and PC can be justified with the presence of discontinuities in the physical space.

We expect that the sTE strategy will perform much more better, with respect the MC and PC methods, if the solution exhibits a non smooth behavior along the stochastic space. In order to clarify the problem at the probe P2, the solution relative to this probe ($x = 0.5$) is reported as a function of the stochastic space in the figure 17 at the final time step. As clearly shown in figure 17, several discontinuities arise in this case in the stochastic space, even if all the solutions of the heat problem are smooth in the physical space, except for the initial conditions.

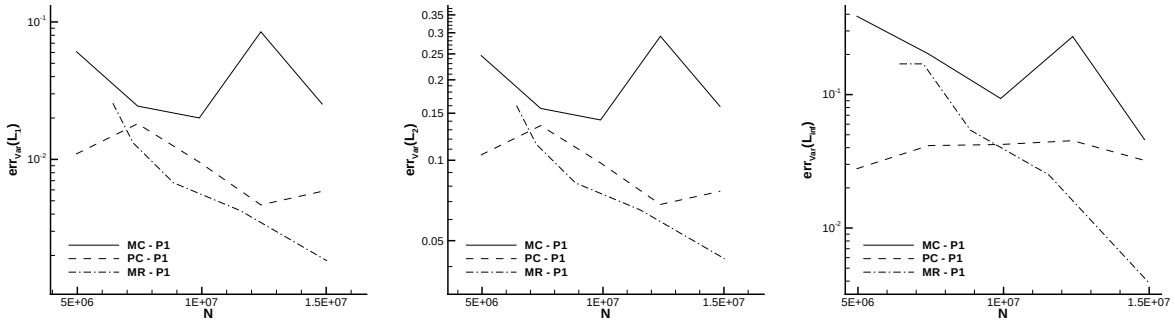

(a) (b) (c)

Figure 14: Error norms of the variance of the variable u, corresponding to the probe P1, for the 1D heat equation problem with uniform pdf in the L_1 (a), L_2 (b) and L_∞ (c) spaces.

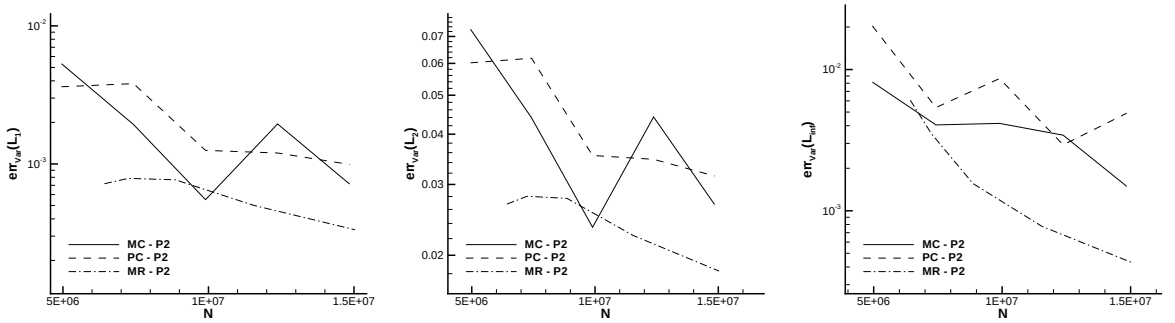

(a) (b) (c)

Figure 15: Error norms of the variance of the variable u, corresponding to the probe P2, for the 1D heat equation problem with uniform pdf in the L_1 (a), L_2 (b) and L_∞ (c) spaces.

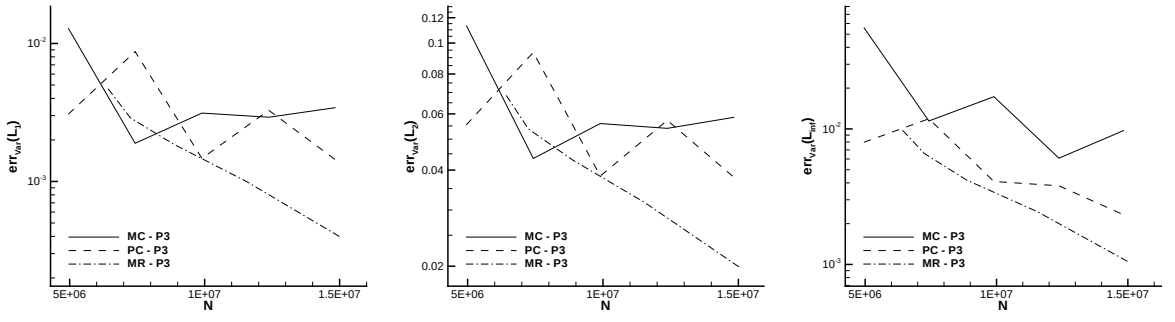

(a) (b) (c)

Figure 16: Error norms of the variance of the variable u, corresponding to the probe P3, for the 1D heat equation problem with uniform pdf in the L_1 (a), L_2 (b) and L_∞ (c) spaces.

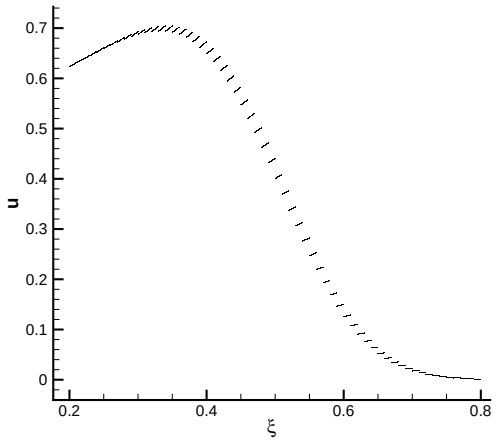

Figure 17: Solution $u(0.5, 0.5, \xi)$ corresponding to the probe P2 at the final time step obtained with 1000 MC samples.

6. Concluding remarks

This paper presents an innovative adaptive strategy for stochastic differential equations, the sTE algorithm, inspired to the classical Harten's framework. A representation of the solution on a finest grid is computed starting from a coarsest one, with a reduced number of function evaluations. As a consequence, only a reduced set of point values on the finest grid is evaluated, while the remaining set is obtained by interpolation (from the previous levels). This procedure moves recursively, with a combination of interpolation and evaluation, from the coarsest level to the finest and from each time step to the successive one. At each time step, the scheme allows to recover the solution on the finest level with a one time scheme that embeds the encoding and the truncation procedures of the classical Harten framework. Afterwards, this strategy is extended to the partial differential equation. A spatial discretization is chosen, as well as the time discretization, in order to solve the deterministic problem with a desired accuracy. The initial condition is discretized on the grid $D \times \Xi$ employing the finest resolution level in the stochastic space and the chosen spatial discretization. Then, the sTE strategy is applied to the associated stochastic space obtaining the MR representation of the solution at each time step, for each spatial node, *i.e.* the representation of the stochastic function obtained at a fixed physical space and time.

The sTE strategy is applied to some "simplified" numerical test-cases and compared to classical stochastic methods. Finally, it is applied to the stochastic heat equation discretized by finite elements and integrated in time by means of a fourth order Runge-Kutta method. A discontinuous initial condition is considered. The sTE displays very promising results in terms of accuracy, convergence and regularity. Future works will focus on the extension of the present strategy to hyperbolic partial differential equations.

Acknowledgements

Remi Abgrall has been partially supported by the ERC Advanced Grant ADDECCO N. 226316, while Gianluca Geraci has been fully supported by the ERC Advanced Grant ADDECCO N. 226316.

References

[1] N. Wiener, The Homogeneous Chaos, American Journal of Mathematics 60 (1938) 897–936.
[2] D. Xiu, G. E. Karniadakis, Modeling uncertainty in flow simulations via generalized polynomial chaos, Journal of Computational Physics 187 (2003) 137–167.
[3] X. Wan, G. E. Karniadakis, Long-term behavior of polynomial chaos in stochastic flow simulations, Computer Methods in Applied Mechanics and Engineering 195 (2006) 5582–5596.

[4] M. Gerritsma, J.-B. van der Steen, P. Vos, G. E. Karniadakis, Time-dependent generalized polynomial chaos, Journal of Computational Physics 229 (2010) 8333–8363.
[5] J. Foo, G. E. Karniadakis, Multi-element probabilistic collocation method in high dimensions, Journal of Computational Physics 229 (2010) 1536–1557.
[6] O. Le Maître, Uncertainty propagation using WienerHaar expansions, Journal of Computational Physics 197 (2004) 28–57.
[7] O. Le Maître, Multi-resolution analysis of Wiener-type uncertainty propagation schemes, Journal of Computational Physics 197 (2004) 502–531.
[8] J. Tryoen, O. Le Maître, M. Ndjinga, A. Ern, Intrusive Galerkin methods with upwinding for uncertain nonlinear hyperbolic systems q, Journal of Computational Physics 229 (2010) 6485–6511.
[9] R. Abgrall, P. M. Congedo, C. Corre, S. Galéra, A simple semi-intrusive method for uncertainty quantification of shocked flows, comparison with a non-intrusive polynomial chaos method, in: V European Conference on Computational Fluid Dynamics ECCOMAS CFD 2010 J. C. F. Pereira and A. Sequeira (Eds) Lisbon, Portugal,14-17 June 2010, June, pp. 1–17.
[10] R. Abgrall, P. M. Congedo, S. Galéra, A semi-intrusive deterministic approach to uncertainty quantifications in non-linear fluid flow problems, Technical Report, INRIA RR-7820, 2011.
[11] R. Abgrall, P. M. Congedo, S. Galéra, G. Geraci, Semi-intrusive and non-intrusive stochastic methods for aerospace applications, in: 4TH EUROPEAN CONFERENCE FOR AEROSPACE SCIENCES, Saint Petersburg, Russia, July 4th-8th, 2011, 1, pp. 1–8.
[12] A. Harten, Adaptive multiresolution schemes for shock computations, Journal of Computational Physics 135 (1994) 260–278.
[13] A. Harten, Multiresolution algorithms for the numerical solution of hyperbolic conservation laws, Communications on Pure and Applied Mathematics 48 (1995) 1305–1342.
[14] A. Harten, Multiresolution Representation of Data : A General Framework, SIAM Journal on Numerical Analysis 33 (1996) 1205–1256.
[15] R. Abgrall, P. M. Congedo, G. Geraci, A One-Time Truncate and Encode Multiresolution Stochastic Framework, Technical Report, INRIA Bordeaux–Sud-Ouest, 2012.
[16] O. Le Maître, O. Knio, Spectral Methods for Uncertainty Quantification: With Applications to Computational Fluid Dynamics, Springer Verlag, 2010.
[17] R. Abgrall, A. Harten, Multiresolution Representation in Unstructured Meshes, SIAM Journal on Numerical Analysis 35 (1998) 2128–2146.
[18] A. Quarteroni, R. Sacco, F. Saleri, Matematica Numerica, Springer, 2008.
[19] A. Quarteroni, Modellistica numerica per problemi differenziali, Springer, 2008.

Appendix A. Finite element discretization of the 1D heat equation

In this section, we want to provide more details about the finite element scheme employed to solve the heat problem (9). For an exhaustive analysis of the problem, the reader may refer to [19].

Let us consider first, how to reduce the problem (9) from the weak form to the algebraic form (11). The weak formulation can be obtained by multiplying the equation (9), for the test function $v \in V$. As a consequence, the equation (10) is computed by integrating over the physical space

$$\int_D \frac{\partial u(x,t,\xi)}{\partial t} v \, \mathrm{d}x = \int_D \nu \frac{\partial^2 u(x,t,\xi)}{\partial x^2} v \, \mathrm{d}x. \tag{A.1}$$

The right-hand side can be decomposed using the integration by parts as follows

$$\begin{aligned} \int_D \nu \frac{\partial^2 u(x,t,\xi)}{\partial x^2} v \, \mathrm{d}x &= \int_D \nu \frac{\partial}{\partial x}\left(\frac{\partial u}{\partial x} v\right) \mathrm{d}x - \int \nu \frac{\partial u}{\partial x}\frac{\mathrm{d}v}{\mathrm{d}x}\mathrm{d}x \\ &= \nu \left[\frac{\partial u}{\partial x} v\right]_0^1 - \int_D \nu \frac{\partial u}{\partial x}\frac{\mathrm{d}v}{\mathrm{d}x}\mathrm{d}x \\ &= -\int_D \nu \frac{\partial u}{\partial x}\frac{\mathrm{d}v}{\mathrm{d}x}\mathrm{d}x, \end{aligned} \tag{A.2}$$

where the test functions are equal to zero at the boundaries ($v(0) = v(1) = 0$) and a Dirichlet boundary condition is applied. The integrals are well-posed if $v \in H_0^1(0,1)$:

$$H_0^1(0,1) = \left\{ v \in H^1(0,1) : v(0) = v(1) = 0 \right\}. \tag{A.3}$$

The problem reduces to search $u \in V = H_0^1(0,1)$

$$\int_D \frac{\partial u(x,t,\xi)}{\partial t} v \, \mathrm{d}x = -\int_D \nu \frac{\partial u}{\partial x}\frac{\mathrm{d}v}{\mathrm{d}x}\mathrm{d}x \quad \forall c \in V. \tag{A.4}$$

The Galerkin approximation of the problem can be obtained by searching for an approximate solution $u_h \in V_h \subset V$, where the space V_h has a finite dimension N_h, with the test functions v in the same space V_h. In the latter case, *i.e.* using the same space for the solution and the tests functions, the approximation is the so-called Bubnov-Galerkin approximation.

If the Lagrangian finite element space is chosen for V_h, the classical basis $\{\phi_i\}$ (in the linear case) is equal to

$$\phi_i = \begin{cases} \dfrac{x - x_{i-1}}{x_i - x_{i-1}} & x_{i-1} \le x \le x_i \\ \dfrac{x_{i+1} - x}{x_{i+1} - x_i} & x_i \le x \le x_{i+1} \\ 0 & \text{otherwise.} \end{cases} \tag{A.5}$$

If the tessellation of the domain is obtained with the nodes $\{x_i\}_{i=0}^{N+1}$, the solution can be expanded as a linear combination of the Lagrangian functions (for all the internal nodes) $u_h(x,t) = \sum_{i=1}^{N} u_i(t)\phi_i(x)$ that, inflated into (A.4), becomes

$$\sum_{i=1}^{N} \int_{D_{ij}} \phi_i \phi_j \mathrm{d}x = -\nu \sum_{i=1}^{N} u_i(t) \int_{D_{ij}} \frac{\mathrm{d}\phi_i}{\mathrm{d}x} \frac{\mathrm{d}\phi_j}{\mathrm{d}x} \mathrm{d}x, \quad \forall \phi_j \in V_h \tag{A.6}$$

where D_{ij} indicates the non-null support of the product function $\phi_i \phi_j$.

If a mass M and a stiffness A matrices are defined as follows

$$\begin{aligned} \mathrm{M} &= \left[m_{ij}\right], \quad m_{ij} = \int_{D_{ij}} \phi_i \phi_j \, \mathrm{d}x \\ \mathrm{A} &= \left[a_{ij}\right], \quad a_{ij} = \int_{D_{ij}} \frac{\mathrm{d}\phi_i}{\mathrm{d}x} \frac{\mathrm{d}\phi_j}{\mathrm{d}x} \mathrm{d}x, \end{aligned} \tag{A.7}$$

the algebraic form (11) can be found as

$$\mathrm{M} \frac{\mathrm{d}\mathbf{U}(\mathbf{t})}{\mathrm{d}t} = -\nu \mathrm{A} \mathbf{U}(\mathbf{t}), \tag{A.8}$$

where the vector $\mathbf{U}(t) = \{u_i(t), \ldots, u_N(t)\}^{\mathrm{T}} \in \mathbb{R}^N$ is the collection of all the degrees of freedom of the linear expansion for $u_h(t)$. The original (9) parabolic partial differential problem is recast in a set of (coupled) ordinary differential equations.

Thanks to the compact support of the Lagrangian basis both M and A have a regular pattern of sparsity. In particular they are symmetric tridiagonal matrices. For recasting the system of ODEs in a set of decoupled ordinary differential equations, the mass matrix can be approximated by a diagonal matrix $\hat{\mathrm{M}}$, *i.e.* the so-called mass lumping technique. Thanks to the properties of the linear Lagrangian element ($\sum_{j=1}^{N} \phi_j = 1$) the mass matrix can be approximated by

$$\hat{\mathrm{M}} = \mathrm{Diag}(\hat{m}_{ii}) \quad \text{with} \quad \hat{m}_{ii} = \sum_{j=1}^{N} m_{ij} = \int_{D_{ij}} \phi_i \sum_{j=1}^{N} \phi_j \, \mathrm{d}x = \int_{D_{ij}} \phi_i \, \mathrm{d}x. \tag{A.9}$$

The lumped matrix becomes $\hat{\mathrm{M}} = \mathrm{Diag}(5/6, 1, \ldots, 1, 5/6)\Delta x$, while for the stiffness matrix we have

$$A = \begin{pmatrix} 2 & -1 & & & \\ -1 & 2 & -1 & & \\ & \ddots & \ddots & \ddots & \\ & & -1 & 2 & -1 \\ & & & -1 & 2 \end{pmatrix} \frac{1}{\Delta x}, \tag{A.10}$$

where we employed a uniform tessellation of the physical space $x_i = i\Delta x$ with $i = 0, \ldots, N+1$ and $\Delta x = 1/N$.

The finite element formulation of the problem is obtained here in the physical 1D case only for the sake of simplicity, but both the deterministic scheme and the sTE strategy, described in 4.3, can be easily extended to physical (and even stochastic) multidimensional cases replacing the mass and stiffness matrices with their multidimensional counterparts and providing a nested set of meshes in Ξ.

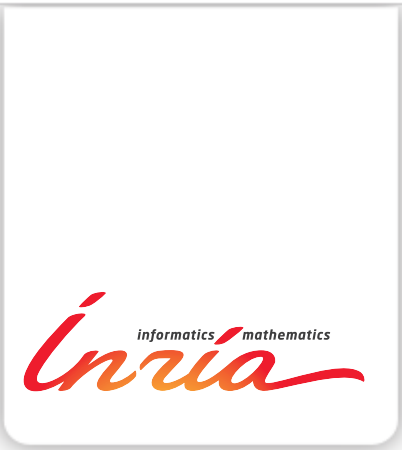

RESEARCH CENTRE
BORDEAUX – SUD-OUEST

351, Cours de la Libération
Bâtiment A 29
33405 Talence Cedex

Publisher
Inria
Domaine de Voluceau - Rocquencourt
BP 105 - 78153 Le Chesnay Cedex
inria.fr

ISSN 0249-6399